Applied Surface Science 494 (2019) 916–928

Contents lists available at ScienceDirect

Applied Surface Science

journal homepage: www.elsevier.com/locate/apsusc

Full length article

Hydrothermal deposition of CoS nanostructures and its multifunctional applications in supercapattery and water electrolyzer

Subramani Surendran[a,b,*], Sathyanarayanan Shanmugapriya[a], Harivignesh Ramasamy[c], Gnanaprakasam Janani[b], Dharmalingam Kalpana[d], Yun Sung Lee[c], Uk Sim[b,**], Ramakrishnan Kalai Selvan[a,**]

[a] Energy Storage and Conversion Devices Laboratory, Department of Physics, Bharathiar University, Coimbatore 641-046, Tamil Nadu, India
[b] Department of Material Science and Engineering, Chonnam National University, Gwangju 61186, Republic of Korea
[c] Department of Chemical Engineering, Chonnam National University, Gwangju 61186, Republic of Korea
[d] CSIR-Central Electrochemical Research Institute-Madras unit, CSIR Madras Complex Taramani, Chennai 600 113, Tamilnadu, India

ARTICLE INFO

Keywords:
Binder-free electrodes
Cobalt sulfide
Electrocatalyst
Supercapattery
Water electrolyzer

ABSTRACT

The development of sustainable energy conversion and storage systems is on demand to ease the energy needs and restrict environmental pollution. Here, we account a unique multifunctional flake-like CoS deposited over the flexible carbon cloth (CoS@CC) by a facile hydrothermal technique. The single-phase hexagonal structured CoS@CC with high crystallinity was identified through the XRD analysis. The morphological feature portrays the uniform distribution of flake-like CoS over carbon cloth. The electrocatalytic properties of the prepared flake-like CoS (CoS@CC) suggests improved electroactivity of requiring minimal overpotentials of 280 mV (OER) and 264 mV (HER) to accomplish a pre-eminent current density of 20 mA cm^{-2}. In addition, a lab-scale water splitting system was projected to achieve a current density of 10 mA cm^{-2} with a low cell voltage of 1.65 V. In view to driving the fabricated water splitting system, a flexible (CoS@CC||rGO) supercapattery was fabricated to deliver an improved specific energy of 38 Wh kg^{-1} at a superior specific power of 533 W kg^{-1}. Therefore, the prepared CoS@CC electrode with improved flexibility, useful catalytic activity, expressive kinetics, and resilient strength serves as a multifunctional material for prospective energy conversion and storage systems.

1. Introduction

The development of nanomaterials is advancing towards high ultimatum owing to the progressive technological modernization. Explicably, the standards of these nanomaterials can be modified by rationalizing its physical nature and sustaining its chemical configurations [1]. Nowadays, conventional nanomaterials are tailored and tuned into ultrafine nanostructures to accomplish alluring intrinsic properties that promote its existence in a wide range of applications [2]. Besides, the evolution of the in-situ growth of these nanostructures over a flexible substrate lends to extend their involvement in the energy conversion and storage (ECS) forum [3]. Eventually, the development of these flexible nanostructures based electrode remains the critical focal point to determine the reputation of these ECS systems. The arising energy and environmental concerns prompt to develop the ECS systems that render the contribution of non-renewable resources and supplies energy in a sustainable manner. The continuous progress of water splitting systems, which is considered an effective conversion system seems to be a textbook solution regarding both energy and environmental concerns [4]. The water splitting systems are a unique system, which entails two electrodes, one acting as a cathode while the other as an anode, inducing the splitting of water into molecular hydrogen and oxygen [5]. Here, the anode facilitates oxygen evolution reaction (OER) which involves four-electron process and functions as the rate-determining step that requires higher overpotential, while the cathode eases with a two-electron process of hydrogen evolution reaction (HER) [6]. This system is capable of producing highly pure hydrogen and oxygen gases without any perilous by-products [7]. The hydrogen gas recognized as a future energy resource for ultimate energy supplies and restricted commotion of eternal fossil fuels [8,9]. Though water splitting seems to be an ideal system, the working electrodes used necessitate the backing of electrocatalysts to overcome a

* Correspondence to: S. Surendran, Energy Storage and Conversion Devices Laboratory, Department of Physics, Bharathiar University, Coimbatore 641-046, Tamil Nadu, India.
** Corresponding authors.
E-mail addresses: surenj503@gmail.com (S. Surendran), usim@jnu.ac.kr (U. Sim), selvankram@buc.edu.in (R.K. Selvan).

https://doi.org/10.1016/j.apsusc.2019.07.162
Received 7 July 2019; Accepted 17 July 2019
Available online 17 July 2019
0169-4332/

specific activation energy barrier called reaction overpotential [10]. These electrocatalysts can either be modified on the surface of the electrode or act as the electrode itself. The primary role of this electrocatalyst is to adsorb reactant intermediates on the surface to form the adsorbed intermediate and thereby facilitates charge transfer between the electrode and reactant [11]. Consequently, the electrocatalysts weaken the reaction overpotential by activating the intermediate chemical transformation. Hence, the electrocatalysts remains a crucial factor to promote the reaction rate and efficiency to confine the energy barrier. Perpetually, the platinum (Pt) and noble metal oxides such as iridium oxide (IrO_2) and ruthenium oxide (RuO_2), is contemplated as a state-of-the-art electrocatalyst for highly efficient HER and OER electroactivity, respectively [12]. These noble metals such as Pt, Ru, and Ir are rarest in the earth's crust and hence, expensive to afford. This criteria largely increments the construction cost of the water-splitting systems and thus, affects its large-scale commercialization [13]. Therefore, a lookout for nature abundant, non-noble transition metal electrocatalysts is highly recommended to promote widespread marketing of the water-splitting systems.

Additionally, the development of energy storage systems serves as a significant backup power source to drive the water-splitting systems mentioned above to give the impression to be an ingenious perception. Considerably, the electrochemical capacitors or supercapacitors are described to be a sustainable energy storage device owing to its swift charging and discharging functions, superior power density (PD), prolonged cycle life, high environmental safety, and rationally economic [14,15]. But, the truncated energy density (ED) response of the supercapacitor seems to be a major setback that desires acquiescence for its improved commercialization [16,17]. To overcome this significant setback, the conventional supercapacitors are hybridized by engaging a non-Faradaic electrode as an anode (negatrode) and the Faradaic electrode as a cathode (positrode) [18]. Therefore, the framed hybrid system is appropriate to be labeled as a supercapattery device since it comprehends with the redox activity to the perception of capacitance [19,20]. Generally, the resolute carbon materials such as 3D carbon nanostructures, porous carbon, reduced graphene oxide (rGO) were commonly recommended as EDLC electrodes that can contribute superior PD and the transition metals featuring multiple redox reactions were carefully chosen as a redox-type material to afford improved ED [19].

Convincingly, both the ECS systems necessitate common non-noble transition metal-based electrode materials to advance its reputation in the commercial arena. Suitably, cobalt-based electrodes have been curiously investigated owing to its ample valence states, interesting electrical conductivity, and natural abundance [21]. Hence, cobalt-based materials are broadly studied and endorsed in great electrochemical activity owing to its resilient strength and kinetics in alkaline electrolytes [22–24]. Recently, cobalt-based sulfides are also gaining high momentum as a viable material in the vast field of ECS systems [25–28]. Cobalt sulfide enhances fast reaction kinetics instigating multiple redox reactions in a broad potential range [21]. Benefitting from the multiple redox reactions, CoS can occupy more electrolytic ions to facilitate improved energy storage capacity, while its diminutive working potential aids earlier electrochemical reaction favoring superior catalytic activity [23]. These cobalt sulfides exist in different stoichiometric ratios like $Co_{1-x}S$, CoS, CoS_2, Co_9S_8, and Co_3S_4, which is alluring interest as a potential electrode material due to its good electrochemical activity, high thermal conductivity, and low cost compared to other metal sulfides [23]. Further, the direct deposition of CoS nanostructures over the substrate can effectively influence the superior electrochemical properties of the CoS. So far, only a few works report the development of CoS directly on CC, but they involve neither more than one step synthesis process nor uses of surfactant to enhance the growth of nanostructures followed by high-temperature thermal treatment. Recently, Liu et al. have demonstrated an electrochemical technique to synthesize CoS nanosheets onto the surface of carbon cloth, and a quick thermal treatment was performed to improve the catalytic performance further. The thermally treated CoS exhibited considerable OER current density (148 mA cm^{-2} at 1.9 V), and excellent durability in continuous measurement for over 12 h [29]. Similarly, Ning et al. presented a two-step electrodeposition strategy for the synthesis of core-shell Co_3O_4@CoS nanosheet arrays on carbon cloth (CC) for supercapacitor applications. Porous Co_3O_4 nanosheet arrays are first directly grown on CC by electrodeposition, followed by the coating of a thin layer of CoS on the surface of Co_3O_4 nanosheets via the secondary electrodeposition. The electrochemical performance demonstrates that the Co_3O_4@CoS/CC possesses a capacitance of 887.5 F g^{-1} at a scan rate of 10 mV s^{-1} (764.2 F g^{-1} at a current density of 1.0 A g^{-1}), and excellent cycling stability (78.1% capacitance retention) at high current density of 5.0 A g^{-1} after 5000 cycles [30]. Likewise, Li et al. established CoS nanosheets vertically grown on carbon cloth (CoS/CC) by using DETA as a surfactant for water splitting over a wide pH range. This material affords a current density of 10 mA cm^2 at a small overpotential of 192 mV and 212 mV in alkaline and acidic media, respectively, along with long-term stability for over 50 h [31]. Xu et al. introduced fabrication of cobalt sulfide (CoS), sulfur-doped Co_3O_4 (S-Co_3O_4), and Co_3O_4 nanomaterials on a carbon cloth substrate by hydrothermal method. The electrochemical result shows that CoS nanomaterial achieved an areal capacitance of 1.98 F cm^{-2} at 2 mA cm^{-2} in a 5 M LiCl solution. Moreover, the CoS has long-term cycling stability with more than 85.7% capacitance retention after 10,000 cycles [32]. Reportedly, Xia et al. proposed a facile method based on anion exchange reactions to achieve metal sulfide nanoarrays through a topotactical transformation from their metal oxide and hydroxide preforms on carbon cloth and nickel foam substrates. The self-supported CoS nanowire arrays are tested as the pseudo-capacitor cathode, which demonstrates enhanced high-rate specific capacities (129 mAh g^{-1} at 2 A g^{-1}) and better cycle life (91% for 3000 cycles) [33]. Though these reports suggest the development of CoS directly on CC, they involve neither more than one step synthesis process nor uses of surfactant to enhance the growth of nanostructures. However, the development of surfactant-free and binder-free facts of flexible CoS@CC nanostructures as a multifunctional electrode material seems to be short to date. Therefore, our strategy is to establish a one-step method to promote uniformly grown nanostructures of CoS over the CC without any pricey surfactants.

Herein, we propose a solitary in-situ deposition of CoS on the carbon cloth (CoS@CC) by a simple one-pot synthesis at a nominal temperature (180 °C). Compared to the reported works, the morphology proposed in this work is completely different, forming a high uniformly fused layer of CoS over the CC. The high uniform growth of the CoS over the CC was emphasized by this method since morphology is the pivotal factor in improving the capacity of the supercapacitors and in enhancing the accessible active surface area of the electrocatalysts. In addition, this solid fusion of CoS over the CC exceedingly enhances the electronic conductivity of the electrode inducing improved electrode kinetics and mass transport. Moreover, this work elucidates the multifunctional capability of the CoS@CC nanostructures, which is not acquainted in reported works. Therefore, the in-situ deposition of CoS over the CC with enhanced surface activity is anticipated as a potential surfactant-free and binder-free flexible multifunctional electrode for the first time to authenticate its potential application in both energy conversion and storage devices.

2. Experimental section

2.1. Materials

All reagents used in the experiments were of analytical grade and were used without further purification. Initially, the fuel cell grade commercial CC was methodically rinsed with conc.HCL for the desertion of partly involved impurities and initiate surface etching. The CoS

nanostructures were carefully deposited over the carbon cloth by a simple in-situ hydrothermal process. Equivalent amounts of cobalt acetate purchased from Himedia and Red phosphorus purchased from Alfa Aesar was isolated in 40 mL of DD water employing a magnetic stirrer to acquire a homogenous mixture. The obtained homogenous mixture was moved to the Teflon-lined autoclave holding the pre-treated CC, sealed tightly, and maintained at 180 °C for 48 h. In the end, the CC with a deposition layer of black nanoparticles was collected and swept away with DD water and ethanol to eliminate residual layers and desiccated. The grown materials were laid open to various investigations.

2.2. Material characterization

The crystal structure and phase formation were analyzed by powder X-ray diffraction (Rint 1000, Rigaku, Japan) with Cu Kα radiation (λ = 1.5418 Å). The morphological features are assessed through the Field-emission scanning electron microscopy (FE-SEM, S-4700, Hitachi, Japan) coupled with energy-dispersive X-ray spectroscopy (EDX) module and high-resolution transmission electron microscopy (HR-TEM; JEM-2000, EX-II, JEOL, Japan). The particle size measurements were measured utilizing Scion Image software. The XPS analysis (Multilab 2000, UK) was used to estimate the active surface elements. The electrocatalytic and electrochemical study was carried out using Bio-Logic VMP3 multichannel electrochemical workstation.

2.3. Electrode fabrication

The prepared CoS over carbon cloth substrate was directly employed as a working electrode for both electrocatalytic and electrochemical studies. Since the decoration of CoS on the carbon cloth was carried out by the in-situ process, the mass of the CC before and after the reaction was measured to estimate the equivalent mass loading of the active material. This measure is used to calculate the specific capacity of the CoS@CC nanostructured electrodes. All the electrochemical performance measurements in this work were carried out in 1 M KOH electrolyte, and Hg/HgO was used as the reference electrodes. Similarly, the graphite electrode was used as the counter for both capacitive and electrocatalytic studies. All potentials reported in the electrocatalytic analysis were against the RHE (Reversible Hydrogen Electrode), which was converted from the Hg/HgO scale using a calibration. The supercapattery device was fabricated by packing CoS@CC as a positrode and rGO as a negatrode separated by a polypropylene sheet as a separator bounded by an aqueous electrolyte (1 M KOH) medium and sealed densely fenced by OHP sheets. The flexible negatrode was prepared by the following methods. The pre-treated commercial carbon cloth was precisely cut into pieces (1 × 1 cm^2) and used as the substrates for the electrochemical activity. The mass of the CC was measured before loading the electrode material. The active material (rGO), carbon black and polyvinylidene difluoride (PVDF) were mixed in the ratio of 8:1:1 with 0.4 mL of *N*-methyl 2-pyrrolidine (NMP). Then the mixture was ground well for an hour to make a homogenous slurry which was coated on the carbon cloth using a paintbrush and dried at 80 °C for overnight in a vacuum oven. Finally, the mass of the CC after loading was measured, and the loading of the active material was precisely optimized to 1 mg per electrode for all the electrochemical activity.

3. Results and discussion

3.1. Structural and morphological analysis

The X-ray diffraction (XRD) analysis helps to determine the structural formation and the phase transparency of the prepared nanostructures. The XRD pattern of the as-prepared CoS (Fig. 1a) shows the strong peaks at 32° and 48° was precisely associated to the (010) and (012) lattice planes of the standard JCPDS data (98-062-4831) authorizing the formation of single-phase hexagonal CoS nanostructures. The prominent sharp and distinct peaks stipulate the crystalline nature of the prepared CoS nanostructures over the carbon cloth. The grain size of the sample was assessed to be around 19 nm by means of the Scherrer's formula [34]. Also, the lattice constants (a = b = 3.3588 Å, c = 5.1695 Å) were calculated with the CELREF software, which is consistent with the testified data of the prepared CoS crystal structure and perceived to possess a cell volume of V = 50.50 × 10^6 pm^3 with a space group of P-mmc (space group number 63). Further, the theoretical specific surface area of the prepared CoS nanostructures is assessed to be 51.08 m^2/g, which was calculated using the equation below [35]:

$$\text{Specific surface area} = \frac{6}{D \times \rho} \quad (1)$$

here 6, D and ρ represents the constant (shape factor), average grain size (in nm) and lattice density (in g/m^3), respectively. Henceforth, the obtained CoS nanoparticles are confirmed to be highly crystalline and phase pure CoS with smaller grain size.

Correspondingly, X-ray photoelectron spectroscopy (XPS) analysis determines the surface properties and chemical valence states of the constituent elements in the surface of the prepared sample. Fig. 1b, c shows the XPS spectra of Co (2p) and S (2p), respectively. The Co 2p spectrum (Fig. 1b) was de-convoluted into six significant components, where the Co $2p_{3/2}$ part at lower binding energies includes three integrant. Explicitly, the one observed at 778.47 eV is ascribed to Co^{3+} species, while the two others located at 781.96, and 787.81 eV corresponds to the Co^{2+} main peak accompanied by its shake-up satellite, respectively [36]. Similarly, the Co $2p_{1/2}$ part of the Co 2p spectrum includes three components at higher binding energies of 792.92, 797.92, and 804.81 eV corresponding to the Co^{3+} species, Co^{2+} main-peak, and its shake-up satellite, respectively [37]. The XPS studies confirm the existence of both Co^{2+} and Co^{3+} cobalt species in the prepared CoS compound, in accordance with which the Co^{3+}/Co^{2+} redox couples are expected to render great potential to undergo sufficient multiple redox reactions to boost the electrochemical performance of the CoS [38,39].

Fig. 1c displays the 2p core-level spectrum of S. The two broad peaks at around 163.08 eV (S $2p_{1/2}$) and 161.78 eV (S $2p_{3/2}$) can be attributed to the sulfur-metal bonds in Co-S and S^{2-} in low coordination on the surface, respectively [37]. The C 1s spectrum of carbon contributed by CC (Fig. 1d) authorizes the strong assembly of the prepared CoS over the CC substrate [40]. The obtained XPS spectra are in good agreement those reports from Xiao et al. and You et al. stating the significance of the presence metallic Co peaks (777 eV–779 eV) in the Co 2p region and the sulfur peak (163 eV–164 eV) in the S 2p region, which is also abridged as a root cause of the synergistic effect that enhances the mass transport favoring improved electrocatalytic activity [41,42].

The FESEM images in Fig. 2 displays the morphological properties of the in-situ grown CoS particles over the carbon cloth. A well-defined, meticulously packed arrangement of flake-like CoS nanostructures on CC was formed, as shown in Fig. 2a–d. The average size of the individual flakes was measured to be around 0.33 μm. Fig. S1 clearly displays the firm deposition of CoS over the CC highlighting the achieved high density of coating by substantially differentiating the coated and uncoated area in the electrode. This elucidates the homogeneously sited CoS nanostructures on the CC. This arrangement was optimized concerning the concentration of the starting materials. According to our previous work, the addition of the starting precursors was adjusted to be 15 mmol appropriately to emulate a controlled orientation of the CoS on CC [43]. As a result, a well-aligned, uniform flake-like CoS were widely erected over the carbon cloth.

Fig. 3 shows the high-resolution transmission electron microscopic (HRTEM) images and elemental mapping images of the prepared sample. Fig. 3a, b represents the low and high magnification images of

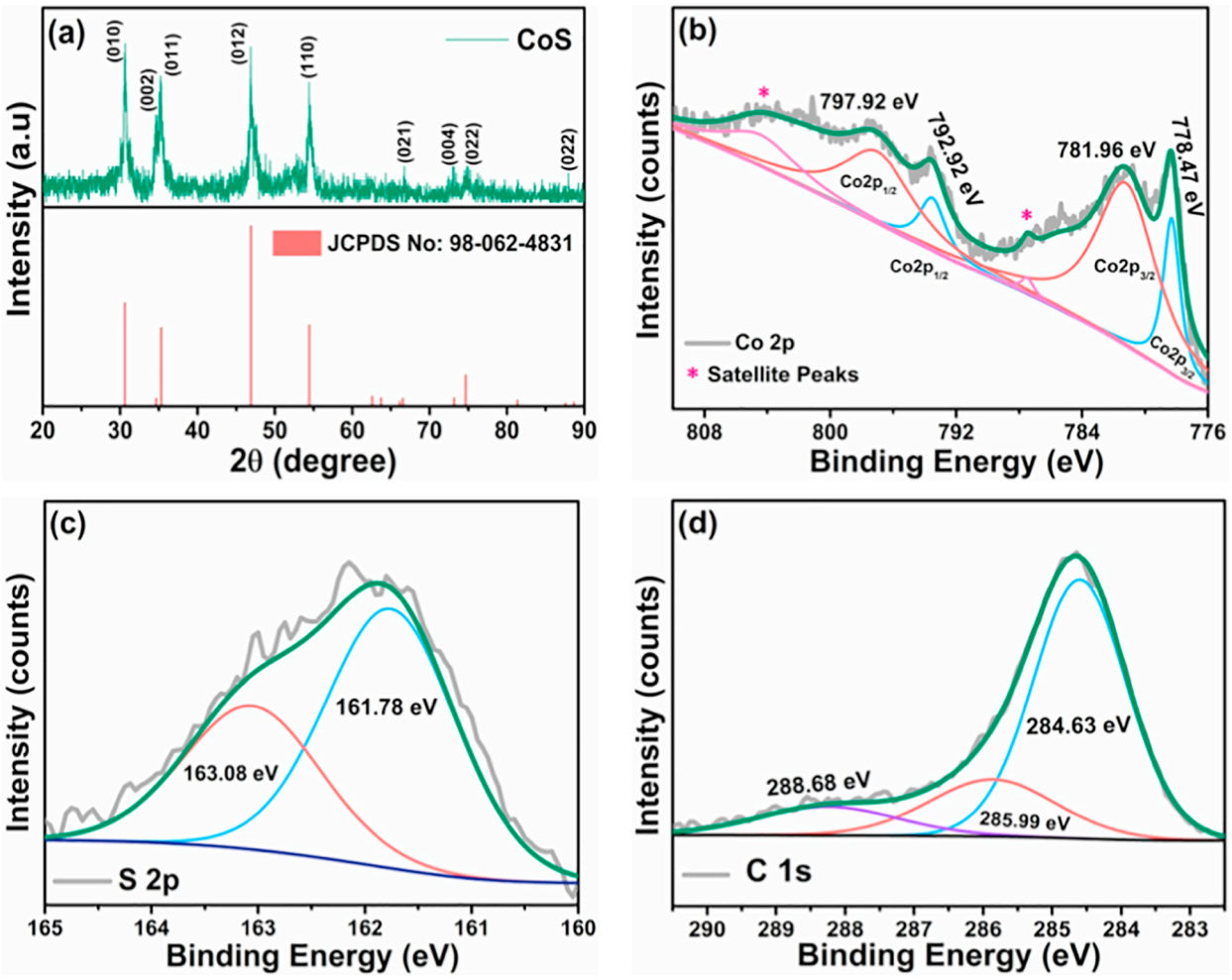

Fig. 1. (a) XRD pattern of CoS@CC with the corresponding JCPDS data, and (b-d) XPS spectra of CoS@CC.

prepared CoS. The HRTEM images in Fig. 3c show distinct lattice fringes with interplanar distances of 0.29 nm corresponding to the (010) plane of the CoS crystal structure. Fig. 3d portrays the SAED pattern that illustrates the polycrystalline nature of the prepared sample. This elucidates that the prepared CoS is in good agreement with the obtained XRD pattern. The elemental mapping images of CoS are shown in Fig. 3e–h, which confirms that the Co, S, and C elements were uniformly distributed in the prepared sample.

3.2. Oxygen evolution reaction

The linear sweep voltammetry (LSV) analysis was examined to evaluate the OER activity of the prepared CoS@CC in addition to ruthenium oxide (RuO_2) and CC electrocatalyst. Fig. 4a shows a sharp peak at 1.1 V (vs. RHE) and a broader peak at 1.4 V (vs. RHE) owing to the oxidation reactions associated to the Co^{2+}/Co^{3+} and Co^{3+}/Co^{4+} redox couples, respectively [44]. The prepared CoS@CC records an exceptional early onset potential at 1.476 V (vs. RHE), which is much higher to that of the ancillary electrocatalysts. Beginning of the onset region, the adsorbed OH^- ions on the surface of the electrode and endures synergistic charge transfer reactions to exfoliate adsorption intermediates. Finally, increasing the applied potential results to evolute massive gas bubbles of oxygen from the surface of the electrode. The flake-like CoS electrocatalyst grown over the CC requisite an overpotential of 280 mV to accomplish a pre-eminent current density of 20 mA cm^{-2}, while the commercial RuO_2 electrocatalysts and CC anticipated essentially higher overpotentials of 301 mV and 406 mV, respectively. The low overpotential demanded by the CoS@CC electrocatalyst explicates its better catalytic activity than the reported CoS@NSCs (380 mV at 10 mA cm^{-2}) [41], CoS_2/N,S-GO (380 mV at 10 mA cm^{-2}) [45], N-Co_9S_8/G (409 mV at 10 mA cm^{-2}) [46], $Co_{0.5}Fe_{0.5}$S@N-MC (410 mV at 10 mA cm^{-2}) [47], CeO_x/CoS (269 mV at 10 mA cm^{-2}) [48], electrocatalysts. Comprehensively, the prepared CoS@CC electrocatalyst was also compared with various Co based electrocatalysts in Table 1 [12,26,49,50].

The superior catalytic activity of the prepared electrocatalysts is accredited to the enhanced structural and morphological orientation of the nanostructure acquired by the facile in-situ technique. Moreover, the CC bears a resemblance to the mesh-like arrangement in which the CoS electrocatalysts are rigidly connected to boost superior conductivity that promotes rapid electron transfer rate. Hence, compared to the conventional electrocatalyst (powder form), the self-standing nanostructures encourages to deliver improved electrocatalytic activity. Fig. 4b exemplifies the essential OER overpotentials of the electrocatalysts to reach different current densities (10 to 50 mA cm^{-2}). This infers that as the potential rises the CoS inclines to demand low overpotentials of 280, 304, 322 and 345 mV at 20, 30, 40, and 50 mA cm^{-2} ensuring a better catalytic activity. Moreover, the better OER catalytic activity of the flake-like CoS@CC was further substantiated with the help of Tafel analysis. The Tafel equation ($\eta = b \log j + a$) was fitted to the Tafel curves of CoS, RuO_2 and CC OER electrocatalyst, to obtain the Tafel slope and is presented in Fig. 4c. From the Tafel analysis, the electrocatalytic activity of CoS electrocatalyst was engrossed by a single electron transfer step with a minimum Tafel slope of 108 mV dec^{-1}.

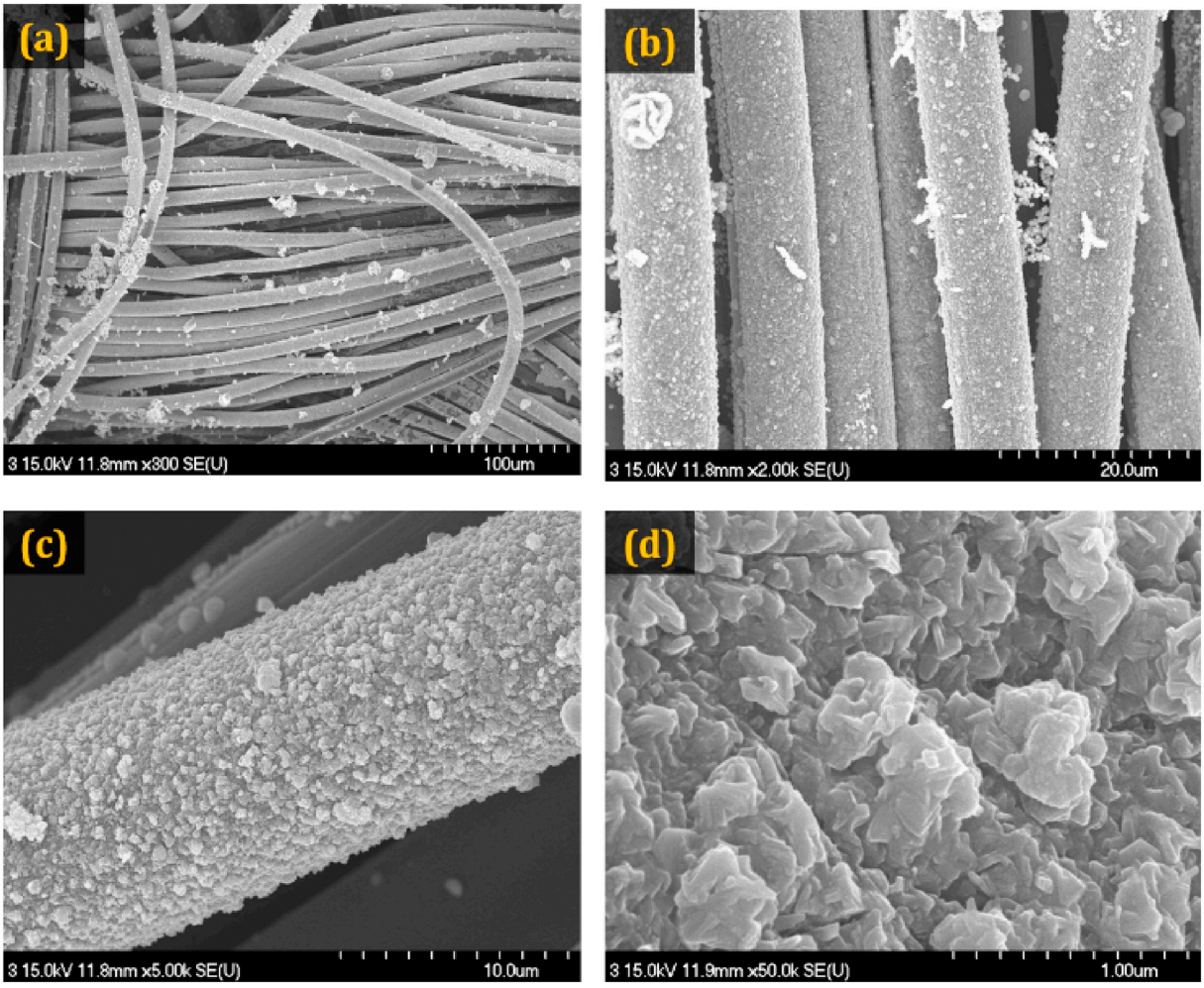

Fig. 2. (a–d) Low and high magnification FESEM images of the prepared flake-like CoS.

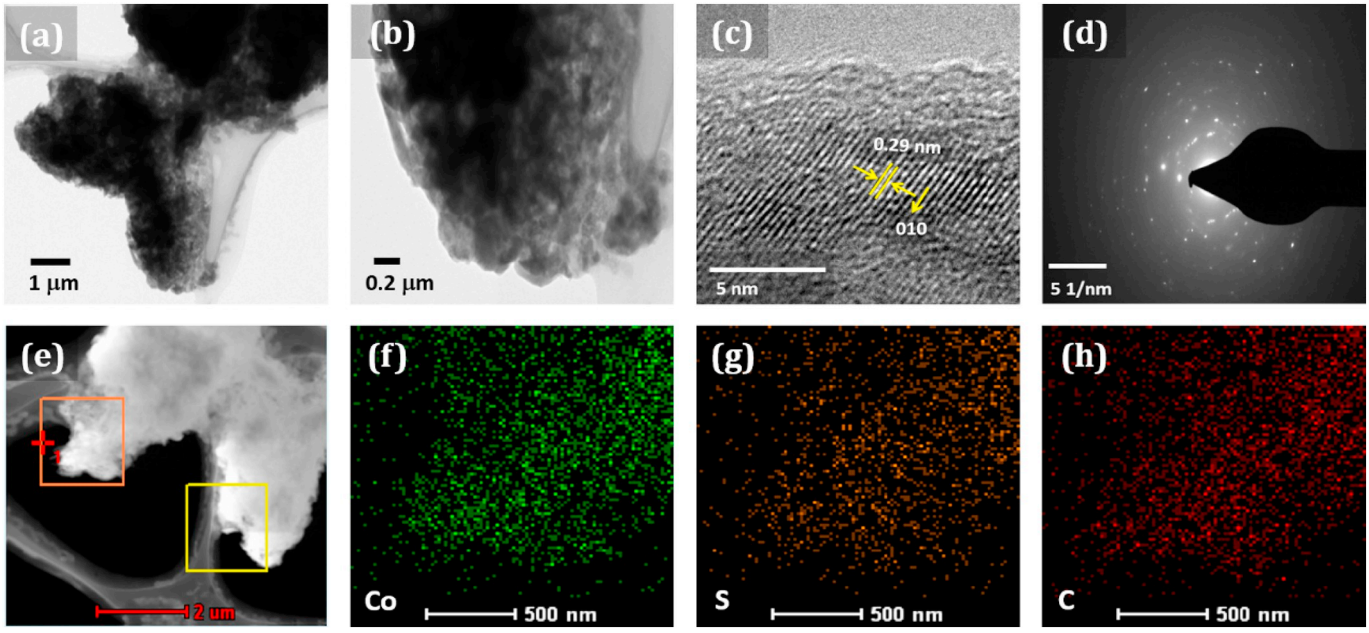

Fig. 3. (a–b) Low and high magnification TEM images, (c) HRTEM image with distinct lattice fringes, (d) SAED pattern and (e–f) Elemental mapping images of the prepared flake-like CoS, respectively.

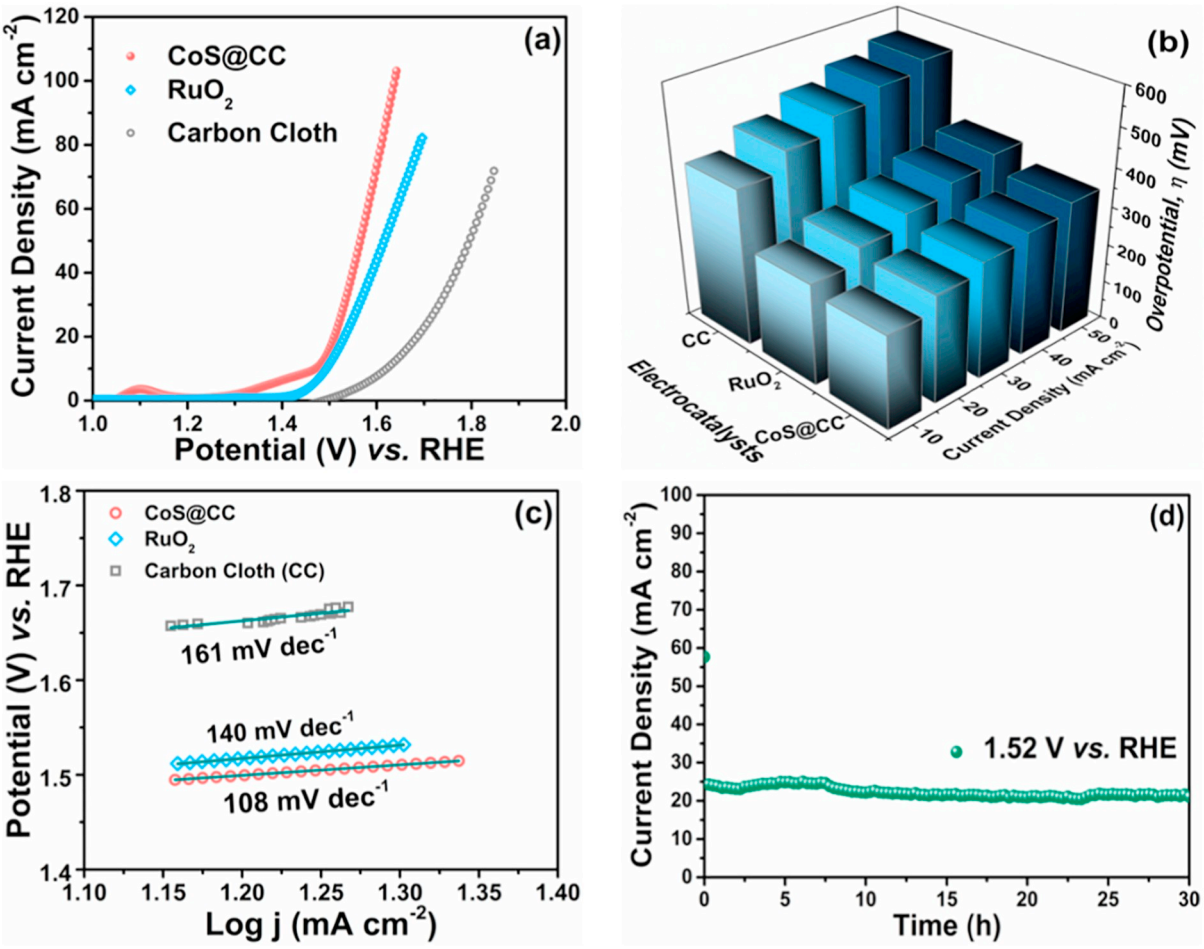

Fig. 4. (a) LSV curves of CoS@CC, RuO_2 and bare carbon cloth for OER, (b) overpotential vs. electrocatalysts to achieve different current densities, (c) OER Tafel plots, and (d) durability curve of CoS@CC electrocatalysts by Chronoamperometry.

Table 1
The OER and HER catalytic activity of the prepared CoS@CC electrocatalysts with other Co-S based electrocatalysts.

Catalyst	OER overpotential [mV] @ 10 mA cm^{-2}	HER overpotential [mV] @ 10 mA cm^{-2}	Ref.
Co_9S_8 ONC	387		[12]
$Co_{9-x}Ni_xS_8$ Octahedral nanocage (ONC)	362		
Ni_9S_8 ONC	374		
Co_9S_8 hollow nanospheres	342	267	[26]
(HNSs)	307	221	
Co_3S_4 HNSs	290	193	
CoS_2 HNSs			
$NiCo_2S_4$ nanowire/NF	260	210	[49]
Co_2B-500	380	328	[50]
Flake-like CoS@CC	243	223	This work

The OER reaction mechanism of the prepared CoS electrode in an alkaline medium can be corroborated with the general mechanism as [51],

$$Co + 2\ OH^- \rightarrow Co(OH)_2 + 2\ e^- \quad (2)$$

$$3\ Co(OH)_2 + 2\ OH^- \rightarrow Co_3O_4 + 4\ H_2O + 2\ e^- \quad (3)$$

$$Co_3O_4 + H_2O + OH^- \rightarrow 3\ CoOOH + e^- \quad (4)$$

$$CoOOH + OH^- \rightarrow CoO_2 + H_2O + e^- \quad (5)$$

$$OER: 4\ OH^- \rightarrow 2\ H_2O + O_2 + 4\ e^- \quad (6)$$

here, Eqs. (2)–(4) substantiates that the active Co species in the CoS@CC electrode are partially oxidized into CoOOH active species and finally forms the CoOOH/CoS hetero-structures as the active sites. These hetero-structures stances as roots to oxidize the absorbed OH^- species into molecular oxygen. At higher applied potential, the so formed CoOOH/CoS intermediate phase gets further oxidized to form CoO_2/CoS (Eq. (5)), an adsorbed secondary transitional phase active species for effective OER activity [52]. Thus, the formation of a thin layer of CoO_2/CoOH shells on the CoS cores ratifies as the constructive, active sites for OER activity [51]. Finally, additional oxidation comprises of desorption of molecular oxygen as air bubbles (Eq. (6)). Here, the in-situ grown CoS over the CC substrate can effortlessly facilitate superior conductivity that favors swift electron transport between the substrate and the catalyst surface, ensuring a faster OER kinetics process compared to the semiconducting cores with very thin CoO_2/CoOH shells as active sites. The chronoamperometry (CA) in Fig. 3d was performed for about 30 h at a persistent potential of 1.52 V (vs. RHE). Providing insignificant current deviations, an interminable production of oxygen bubbles over the surface of CoS@CC was noticeable throughout the CA analysis, and the CoS electrocatalyst owes to ensure its high stability for OER activity. In addition, the FESEM, XPS, and XRD analysis were carried out after long term OER activity to uncover the changes in the morphology, chemical states, and structure of the electrocatalysts (Fig. S2a–b). The FESEM images after OER activity in Fig. S2b portrays no obvious changes in the morphology of the CoS@CC after CA, signifying the resilient long-term OER durability of the

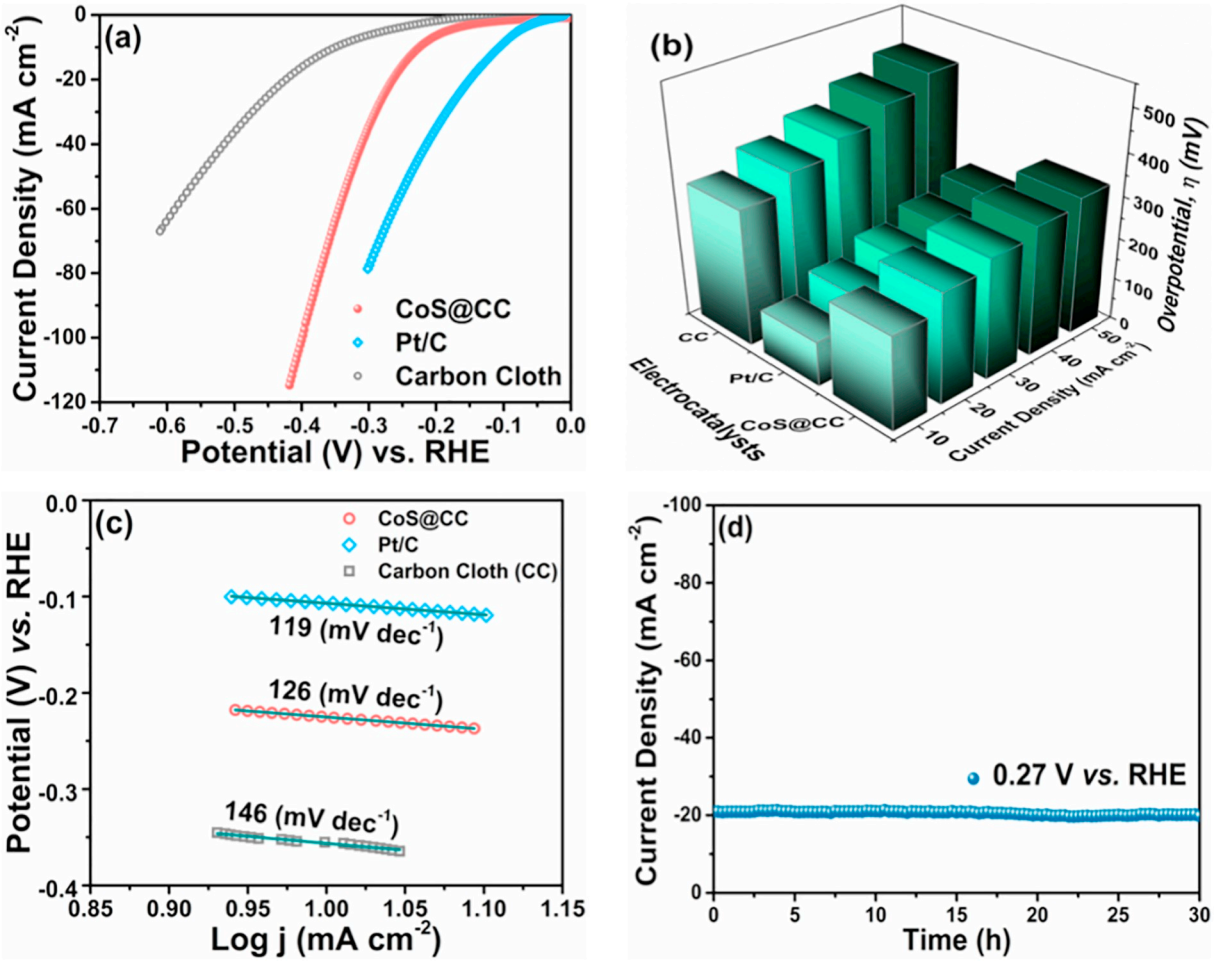

Fig. 5. (a) LSV curves of CoS@CC, Pt/C and bare carbon cloth for HER, (b) the needed overpotential to reach altered current densities, (c) HER Tafel plots, and (d) chronoamperometry of CoS@CC.

prepared electrocatalyst. The Co 2p XPS spectra in Fig. S3 discovers a positively shifted peak of Co $2P_{3/2}$ at 781 eV owing to the surface oxidation of the active Co species in CoS after OER activity. Correspondingly, the XRD pattern in Fig. S4 couldn't perceive any noticeable changes affirming the formation of a very thin oxide layer in the surface of the bulk CoS. This elucidates the proposed catalytic mechanism that suggested the existence of the major phase of CoS inside during OER activity. The overall OER catalytic activity of the CoS@CC electrocatalysts can be accredited to the active Co species in the sulfide. Besides, the flake-like arrangement of CoS nanostructures on CC relish with a superior surface roughness that creates more active sites enhancing the efficiency of the OER activity [53,54].

3.3. Hydrogen evolution reaction

Similarly, the linear sweep voltammetry (LSV) analysis was examined to evaluate the HER activity of the prepared CoS@CC in addition to commercial platinum carbon electrocatalyst (Pt/C 10%) and CC. Fig. 5a shows that the flake-like CoS electrocatalyst grown over the CC shows an exceptional catalytic activity by initiating an onset potential at 0.156 V (vs. RHE).

The prepared CoS electrocatalyst requests an overpotential of 264 mV to accomplish an eminent current density of 20 mA cm^{-2}. Associated to the state of the art commercial Pt/C (149 mV) electrocatalyst, the overpotential necessitated by the prepared CoS@CC electrocatalysts seems to be reasonably comparable to reach alike current density. Compared to the reported CoS_x@NF (240 mV at 10 mA cm^{-2}) [54], Ni_3S_2@NF (269 mV at 10 mA cm^{-2}) [54], Co_3S_4 (270 mV at 10 mA cm^{-2}) [55], Co_9S_8(NS/rGO-Co) (193 mV at 10 mA cm^{-2}) [56], electrocatalysts, the prepared CoS@CC electrocatalyst requested a low overpotential evidencing its improved catalytic activity (Table 1) [26,49,50]. As pronounced formerly, the improved HER electrocatalytic performance of the prepared electrocatalyst is owed to the preparation technique, which induced an improved electron transfer rate between the catalyst and the current collector. Moreover, considering the high magnification FESEM image in Fig. 2c, d, the visible patch-like flakes of CoS holds dynamic surface roughness is generating highly active hydride-acceptor sites on the surface that improves the mass transport profoundly easing the release of hydrogen-air bubbles. Fig. 5b exemplifies the essential HER overpotentials for the electrocatalysts to reach different intervals of current densities (10 to 50 mA cm^{-2}). The prepared CoS@CC requisites a low overpotential of 327 mV to accomplish an improved current density (50 mA cm^{-2}) ensuring a better catalytic activity even at the applied high potential value. The rate determining step of CoS electrocatalyst for HER catalytic activity is obtained from the Tafel analysis (Fig. 5c). From the obtained low Tafel slope of 126 mV dec^{-1}, the rate-determining step is apparently considered as a discharge reaction since the adsorption of hydrogen involves high energy barrier on water dissociation making it a kinetically sluggish phenomenon [57,58]. The CA analysis (Fig. 5d) carried out with a steady potential of −0.27 V (vs. RHE) for 30 h witnesses an eminent strength towards the durability of the CoS@CC electrocatalyst with a nearly constant current and continuous evolution of gas bubbles all through the CA analysis. The post-HER FESEM in Fig.

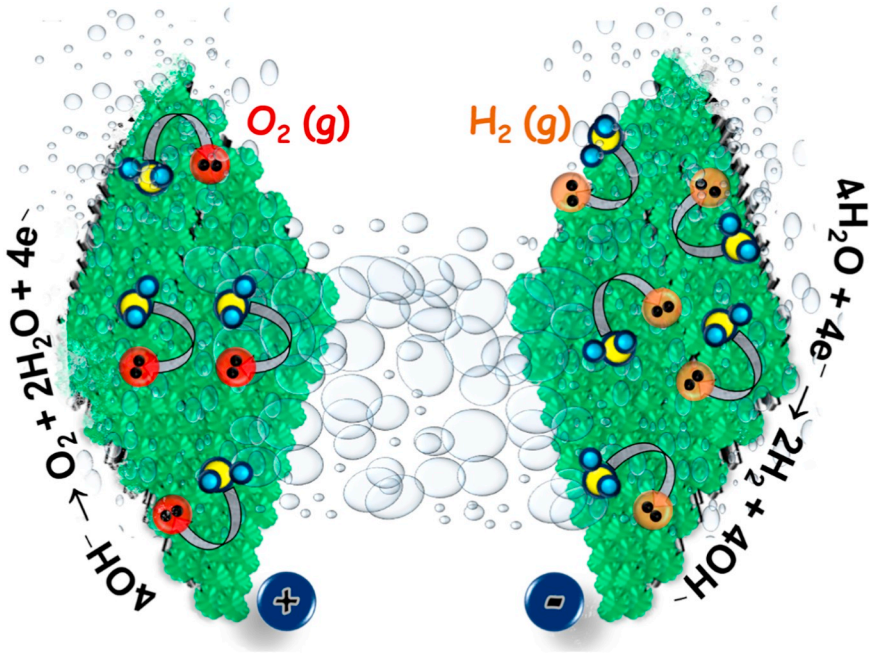

Scheme 1. A typical outline of the fabricated water splitting system.

S2c reveals that no significant changes were perceived in the morphology of the CoS@CC after CA, signifying the resilient long-term OER durability of the prepared electrocatalyst.

3.4. Fabrication of lab-scale water splitting system

Based on the upgraded bifunctional electrocatalytic activity and determined durability, a lab-scale water splitting system was assembled using the prepared CoS@CC as a bifunctional electrocatalyst electrode at both anode and cathode (Scheme 1) [5]. From the respective LSV curve of the designed flexible water-splitting system (Fig. 6a), significant water splitting current density of 10 mA cm^{-2} was achieved with a nominal cell potential of 1.65 V. As a result, the evolution of molecular O_2 and H_2 bubbles were noted at the anode and cathode, respectively.

The CA analysis (Fig. 6b) of the assembled water-splitting system provides a stable trajectory inducing the resilient bifunctional activity of the CoS@CC electrodes at a persistent cell potential of 1.80 V for 30 h. Henceforth, the bifunctional catalytic activity of the prepared CoS@CC bifunctional electrode was established by the remarkable efficiency and determined strength of assembled lab-scale water splitting system.

3.5. Electrochemical activity of CoS@CC as positrode

The cyclic voltammetry (CV) analysis was investigated by a three-electrode system to recognize the electrochemical activity of the prepared CoS@CC electrode in a 1 M KOH electrolyte [59]. The cyclic voltammetry (CV) curves in Fig. 7a shows the performance of the CoS@CC electrode in a working potential of 0 to 0.55 V (vs. Hg/HgO) at various scan rates (1 to 10 mV s^{-1}). The CV curves display a pair of prominent redox peaks sustaining the execution of redox performance of the prepared CoS@CC electrode [60]. The identical activities of the anodic and cathodic peaks substantiate to the rescindable nature of the electrode.

The observable redox peaks at 0.17/0.16 V and 0.50/0.48 V (vs. Hg/HgO) are observed owing to the distinctive oxidation of Co^{2+}/Co^{3+} to Co^{3+}/Co^{4+} state and the same reduction of Co^{4+}/Co^{3+} to Co^{3+}/Co^{2+}

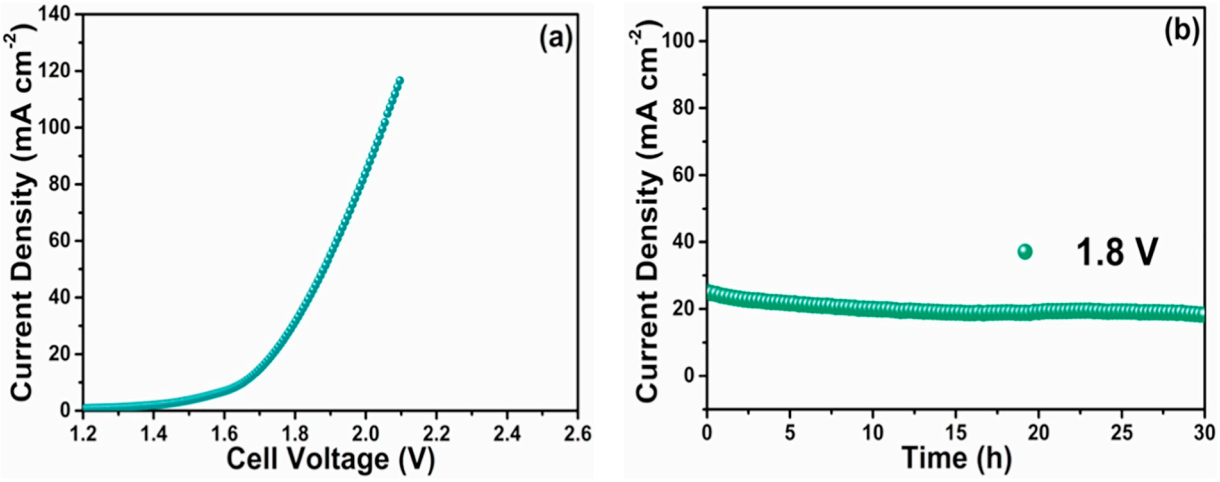

Fig. 6. (a) LSV curves, and (b) chronoamperometry of CoS@CC water splitting cell.

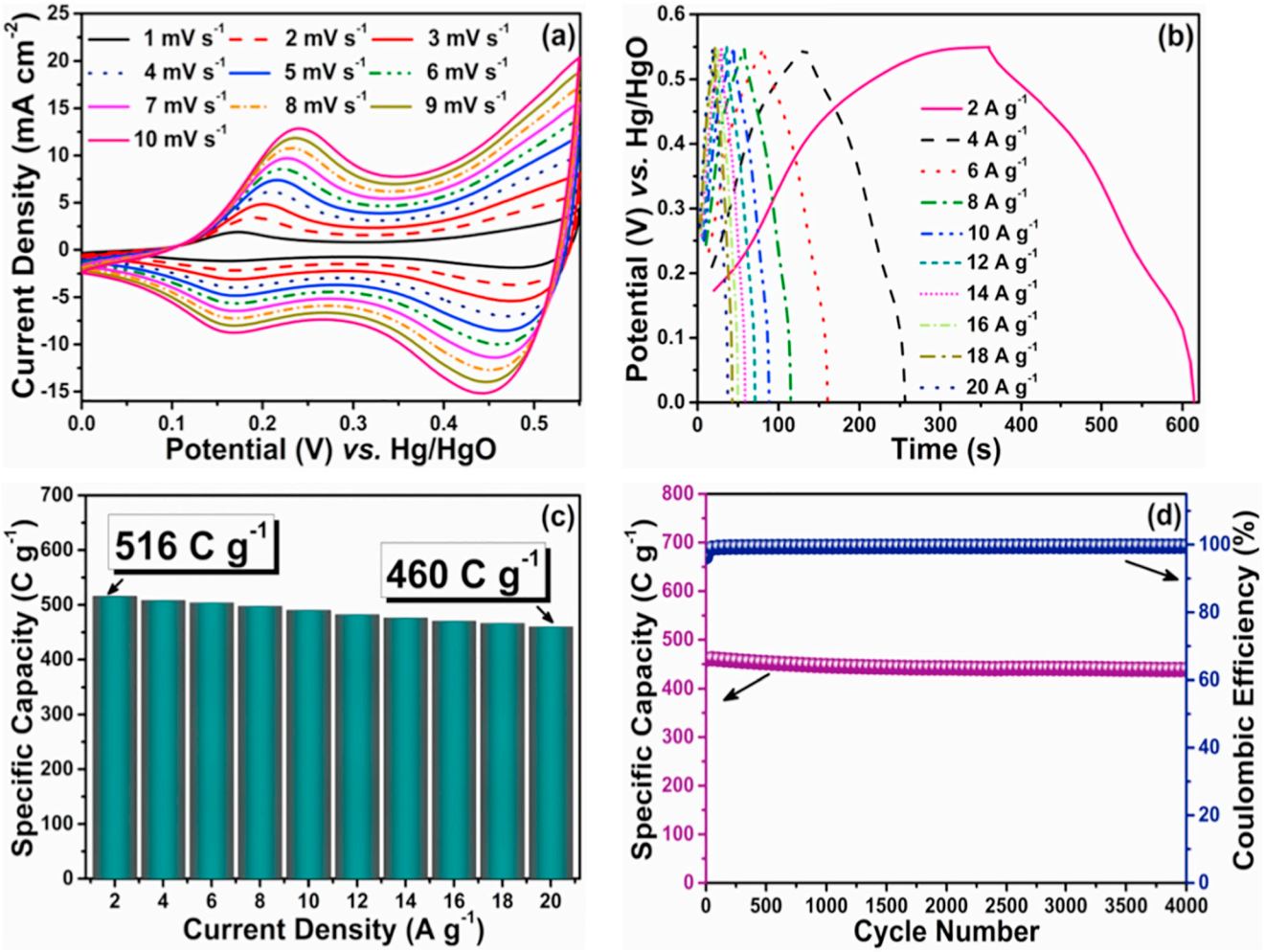

Fig. 7. (a) CV curves of CoS@CC electrode at different scan rates, (b) GCD curves of CoS@CC electrode at different current densities, (c) current density with respect to the specific capacity plot of the CoS@CC electrode, and (d) cycling stability curve of the CoS@CC electrode for 4000 cycles.

reactions, respectively [44]. The electrochemical reaction of CoS@CC electrode can be described as [59],

$$CoS + 2OH^- \longleftrightarrow CoS(OH^-)_2 + 2e^- \quad (7)$$

An improved specific capacitance value of 1077 F g^{-1} at a scan rate of 1 mV s^{-1} is calculated from the CV curves of the CoS@CC electrode. Fig. S5 reveals that the peak current gradually increases with respect to the square root of the scan rate elucidating the complete reaction process is contributed by controlled diffusion [60,61]. A linear equation ($Y = A + (B \times X)$) was fitted with respect to the peak current in accordance with the square root of scan rates, achieved adjacent R^2 value of 0.995 affirming its reaction mechanism. The galvanostatic charge-discharge (GCD) curves of the prepared CoS@CC electrode were shown in Fig. 7b.

The obtained GCD curves with different current densities (2–20 A g^{-1}) in the working potential (0 to 0.55 V (vs. Hg/HgO)) of the electrode clearly visuals the formation plateau region agreeing to the CV curve. This authenticates the battery-type activities of the prepared CoS@CC electrode [59]. The prepared CoS electrode distributed a high specific capacity of 516 C g^{-1} (937 F g^{-1}) at an improved current density of 2 A g^{-1}, which seems to be significantly superior to the reported CoS quasi-spherical nanoparticles (232.6 F g^{-1} at 2 A g^{-1}) [62], flower-like CoS (280 F g^{-1} at 2 A g^{-1}) [63], $Ni_{1.5}Co_{1.5}S_4$ interconnected nanoparticle (1093 F g^{-1} at 1 A g^{-1}) [64], Co/Ni/S spherical (954.3 F g^{-1} at 1 A g^{-1}) [65]. The current density versus specific capacity plot represented in Fig. 7c shows that only 11% of the initial capacity of the electrode was lost after a considerable current density of 20 A g^{-1}. To comprehend the cycle life of the electrode material, the cyclic stability test was performed for about 4000 cycles at a standing current density of 20 A g^{-1} (Fig. 7d). The prepared CoS electrode has shown improved performance by rationally losing 10% of its initial specific capacity, endorsing the sturdy nature of the CoS@CC electrode in 1 M KOH alkaline electrolyte. The FESEM image of CoS/CC electrode after cycle stability test discloses that not any significant changes were observed in the morphology, enlightening the long-term stability of the prepared electrocatalyst (Fig. S2d). Fig. S6 shows the Nyquist plot obtained for the prepared COS@CC electrode. The CoS@CC electrode revealed a small semicircle in the high-frequency region, demonstrating the confined resistance between the electrode and electrolyte. The impedance plot was fitted with an equivalent circuit (inset of Fig. S6 and Table S1) to acquire the corresponding low R_s (1.23 Ω) and R_{ct} (0.313 Ω) values. These results confirm the high conductive nature of the working electrode that reassures fast charge transfer kinetics [66]. The angle of the tail of the semicircle is approached to be around 45° validating the superior ionic passage and the ideal capacitor behavior of the CoS@CC [67]. The perceived results anticipate that the prepared CoS@CC electrode was demonstrated as a reputable positrode with enriched flexibility for the commercial supercapattery application.

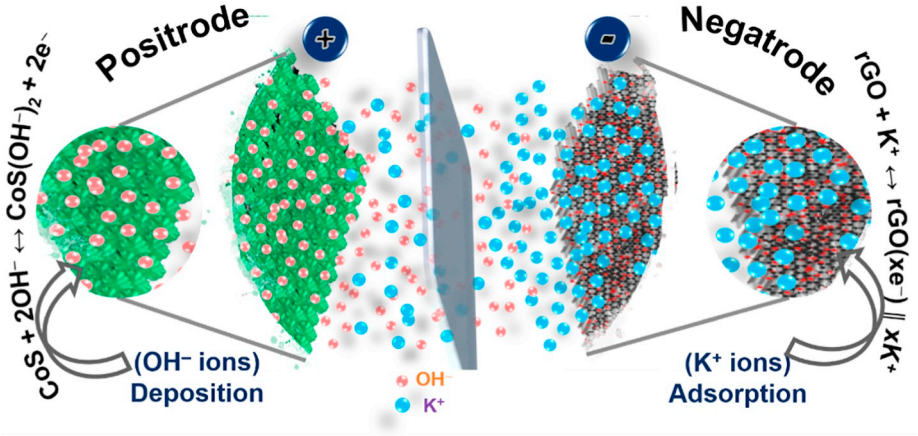

Scheme 2. Charging/discharging mechanism of fabricated CoS@CC||rGO supercapattery.

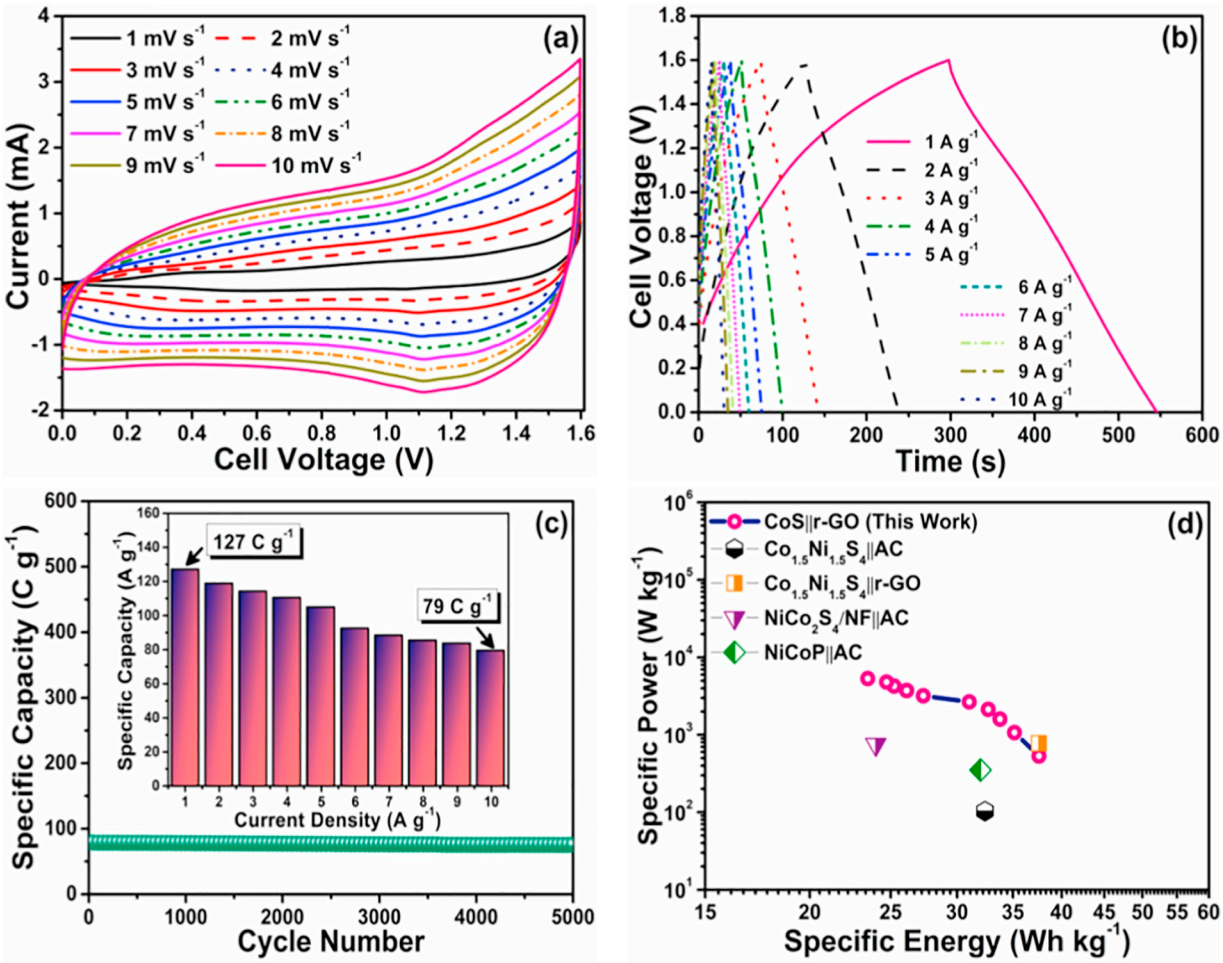

Fig. 8. (a) CV curves of fabricated supercapattery at diverse scan rates, (b) GCD curves of the supercapattery at several current densities, (c) cyclic stability curve (5000 cycles), (inset) current density vs capacity plot of the device and (d) Ragone plot of the CoS@CC||rGO device compared to similar asymmetric device.

3.6. Electrochemical properties of fabricated (CoS@CC||rGO) supercapattery

Encouraging investigation of the flake-like CoS@CC as a positive electrode, a model aqueous supercapattery device was assembled. As represented in the schematic diagram (Scheme 2), the CoS@CC (positrode) and rGO (negatrode) were wrapped densely in an aqueous electrolyte medium [59]. The fabricated device was scrutinized by obtaining the CV and GCD curves in a broad operating cell potential (0 to 1.6 V). Fig. 8a, b shows the obtained CV and GCD curves of the device. From the GCD curve, the specific capacity of the device was calculated as 127 C g^{-1} at a significant current density of 1 A g^{-1}.

Later, a comparable initial specific energy of 38 Wh kg^{-1} at a specific power of 533 W kg^{-1} was succeeded by the designed system at a current density of 1 A g^{-1}. The assembled system grasped an ultimate specific energy value value of 24 Wh kg^{-1} at a substantial specific power of 5333 W kg^{-1}. Fig. 8c shows the cyclic life of the assembled device, which displays a linear trajectory of a straight streak,

Table 2
Comparative performance analysis of fabricated CoS@CC||rGO supercapattery with other asymmetric supercapacitors.

Device materials	Substrate used	Electrolyte	Cell voltage (V)	Specific capacitance	ED (Wh kg^{-1})	PD (W kg^{-1})	Ref. no.
$Co_{1.5}Ni_{1.5}S_4$ ||AC	Nickel foam (NF)	2 M KOH	1.6	–	32.4 & 25	103.4 & 5500	[62]
$Ni_{1.5}Co_{1.5}S_4$||rGO	Nickel foam (NF)	6 M KOH	1.6	113 F g^{-1} at 1 A g^{-1}	37.6 & 23.25	775 & 17,700	[64]
Ni/Co/S-1||AC	Nickel foam (NF)	3 M KOH	1.45	100.4 F g^{-1} at 1 A g^{-1}	29.3 & 13.4	700 & 7400	[65]
Co_3S_4||Co_3S_4-rGo	Nickel foam (NF)	PVA-KOH gel	1.5	–	1.09 & 0.31	398 & 750	[68]
$NiCo_2S_4$/NF||AC	Nickel foam (NF)	2 M KOH	1.5	111.3 F g^{-1} at 1 A g^{-1}	34.7 & 17.9	750 & 15,000	[69]
NiCoP||AC	Nickel foam (NF)	6 M KOH	1.6	164 C g^{-1} at 0.5 A g^{-1}	32 & 18	351 & 5586	[70]
CoS@CC||rGo	CC	1 M KOH	1.6	127 C g^{-1} at 1 A g^{-1}	38 & 24	533 & 5333	This work

substantially holding a persistent capacity for about 5000 successive cycles. The current density vs. specific capacity plot of the device in the inset of Fig. 8c displays the better capacity retention behavior of the device by maintaining 62% of its capacity from 1 A g^{-1} to 10 A g^{-1}. The respective Ragone plot of the fabricated CoS@CC||rGO supercapattery compared to the reported asymmetric devices is shown in Fig. 8d. The thorough evaluation of comparable hybrid devices is tabularized in Table 2 [62,64,65,68–70]. Scheme 2 demonstrates the function of the fabricated supercapattery device. When a potential is applied to the device, the positive potential at the positrode draws all the possible oppositely OH^- ions. These OH^- ions noticeably deposits over the CoS electrode surface by the influential redox reaction as follows [14],

$$CoS + 2OH^- \rightarrow CoS(OH^-)_2 + 2e^- \quad (8)$$

Instantaneously, the negative potential at the negatrode all the possible positive K^+ ions drawn towards the rGO electrode surface. These K^+ ions are held by the rGO electrode due to an electrostatic force establishing EDLC behavior as follows [14],

$$rGO + K^+ \rightarrow rGO(xe^-)\|xK^+ \quad (9)$$

Hence, the potential is stowed in a resourceful means by integrating the redox and EDLC activities. The stored potentials are inhibited by an external load.

The discharge process comprises dissolution and the desorption of negative (OH^-) and positive (K^+) ions from the CoS@CC and rGO electrodes, respectively as [14],

$$CoS(OH^-)_2 + 2e^- \rightarrow CoS + 2OH^- \quad (10)$$

$$rGO(xe^-)\|xK^+ \rightarrow rGO + K^+ \quad (11)$$

Confirming the high repute of the rate capability property and cyclic stability, the fabricated device can be subjected to several charges and discharge cycles. Moreover, the key effect to the enhanced ED was accredited to the uniform distribution of the active material over the knitted structure carbon cloth substrate, which provides adequate room for the fast ions transferences. Thus, a supercapattery system acquainting with advanced ED relating to the higher PD was recognized to reinforce its exploit for commercial purpose.

Overall, the improved electrocatalytic and electrochemical performance of the flake-like CoS grown on the CC is mainly accredited to its (i) uniform morphology, (ii) perpetual arrangement, and (iii) the unique electrochemical and electrocatalytic properties of the prepared CoS@CC. Briefly, the FESEM images reveal the uniform flake-like particles of CoS over the CC possessing irregular edges. This irregularity paves the way for activating additional active sites, providing more room for electrolytic ions to get accumulated on the electrode surface instigating both electrochemical and electrocatalytic activity. Secondly, the perpetual arrangement of the CoS particles over the carbon cloth resembles a closely packed mesh-like electrode. This arrangement eases the in-depth accessibility of the electrolytic ions creating improved electrochemical surface area and electrical conductivity, which is a crucial factor to attain superior electrocatalytic and electrochemical activity. Lastly, the characteristic earlier electrochemical activity and multiple redox behaviors of the Co species that liberates sufficient free electrons, subsequently increases the electrical conductivity, kinetic rate, and rate capability [21–23]. Thus, an improved electrode material was recognized by means of a simple one-step in-situ hydrothermal method to benefit both energy storage and conversion systems.

4. Conclusions

A unique multifunctional flake-like CoS electrode is developed over the flexible carbon cloth (CoS@CC) by a facile in-situ hydrothermal technique. The crystalline and single-phase formation of hexagonal structured CoS is confirmed through XRD analysis. The surface analysis of the prepared CoS was examined by XPS analysis. The morphological features portraying the flake-like CoS were obtained through the SEM micrographs. The flake-like CoS@CC was subjected to the electrocatalytic activity where it demands minimal overpotentials of 280 mV (OER) and 264 mV (HER) to reach a pre-eminent current density of 20 mA cm^{-2}. Further, a lab-scale water splitting system was assembled delivering a perceptibly essential current density of 10 mA cm^{-2} from a truncated cell voltage of 1.65 V, which is compatible enhanced by providing additional flexibility and resilient durability. A flexible (CoS@CC||rGO) supercapattery was fabricated, providing an improved ED of 38 Wh kg^{-1} at a PD of 533 W kg^{-1}. In the future, the multifunctional ability of the binder-free flake-like CoS@CC electrode can be authorized by its credible application in both energy storage and conversion devices.

Acknowledgment

S.S. would like to thank Bharathiar University for providing the University Research Fellowship (URF). Prof. Y.S. Lee and Prof. Uk Sim greatly acknowledges the National Research Foundation of Korea (NRF) grant funded by the Korea government (Ministry of Science, ICT & Future Planning) (2019R1A4A2001527, 2018R1C1B6001267, and 2018R1A5A1025224), respectively.

Appendix A. Supplementary data

Supplementary data to this article can be found online at https://doi.org/10.1016/j.apsusc.2019.07.162.

References

[1] M.A. El-Sayed, Small is different: shape-, size-, and composition-dependent properties of some colloidal semiconductor nanocrystals, Acc. Chem. Res. 37 (2004) 326–333.
[2] J. Nai, X.W. Lou, Hollow structures based on Prussian blue and its analogs for electrochemical energy storage and conversion, Adv. Mater. (2018), https://doi.org/10.1002/adma.201706825 1706825.
[3] K.V. Sankar, Y. Seo, S.C. Lee, S.C. Jun, Redox additive-improved electrochemically and structurally robust binder-free nickel pyrophosphate nanorods as superior cathode for hybrid supercapacitors, ACS Appl. Mater. Interfaces 10 (2018) 8045–8056.
[4] C. Ray, S.C. Lee, K.V. Sankar, B. Jin, J. Lee, J.H. Park, S.C. Jun, Amorphous phosphorus-incorporated cobalt molybdenum sulfide on carbon cloth: an efficient and stable electrocatalyst for enhanced overall water splitting over entire pH values, ACS Appl. Mater. Interfaces 9 (2017) 37739–37749.

[5] A. Sivanantham, P. Ganesan, L. Estevez, B.P. McGrail, R.K. Motkuri, S. Shanmugam, A stable graphitic, nanocarbon-encapsulated, cobalt-rich core-shell electrocatalyst as an oxygen electrode in a water electrolyzer, Adv. Energy Mater. 8 (2018) 1702838.

[6] Y. Ji, L. Yang, X. Ren, G. Cui, X. Xiong, X. Sun, Full water splitting electrocatalyzed by $NiWO_4$ nanowire array, ACS Sustain. Chem. Eng. 6 (2018) 9555–9559.

[7] L. Ai, J. Su, M. Wang, J. Jiang, Bamboo-structured nitrogen-doped carbon nanotube coencapsulating cobalt and molybdenum carbide nanoparticles: an efficient bifunctional electrocatalyst for overall water splitting, ACS Sustain. Chem. Eng. 6 (2018) 9912–9920.

[8] T.S. Dörr, L. Deilmann, G. Haselmann, A. Cherevan, P. Zhang, P. Blaha, P.W. de Oliveira, T. Kraus, D. Eder, Ordered mesoporous TiO_2 gyroids: effects of pore architecture and Nb-doping on photocatalytic hydrogen evolution under UV and visible irradiation, Adv. Energy Mater. 8 (2018) 1802566.

[9] J. Mahmood, M.A.R. Anjum, S.-H. Shin, I. Ahmad, H.-J. Noh, S.-J. Kim, H.Y. Jeong, J.S. Lee, J.-B. Baek, Encapsulating iridium nanoparticles inside a 3D cage-like organic network as an efficient and durable catalyst for the hydrogen evolution reaction, Adv. Mater. 30 (2018) 1805606.

[10] M.R. Pai, A.M. Banerjee, A.K. Tripathi, S.R. Bharadwaj, Fundamentals and applications of the photocatalytic water splitting reaction, Funct. Mater. (2012) 579–606, https://doi.org/10.1016/B978-0-12-385142-0.00014-3 (Elsevier).

[11] Y. Pan, H. Ren, H. Du, F. Cao, Y. Jiang, H. Du, D. Chu, Active site engineering by surface sulfurization for a highly efficient oxygen evolution reaction: a case study of Co_3O_4 electrocatalysts, J. Mater. Chem. A 6 (2018) 22497–22502.

[12] J. Kim, H. Jin, A. Oh, H. Baik, S.H. Joo, K. Lee, Synthesis of compositionally tunable, hollow mixed metal sulphide $Co_xNi_yS_z$ octahedral nanocages and their composition-dependent electrocatalytic activities for oxygen evolution reaction, Nanoscale 9 (2017) 15397–15406.

[13] J. Li, Y. Wang, T. Zhou, H. Zhang, X. Sun, J. Tang, L. Zhang, A.M. Al-Enizi, Z. Yang, G. Zheng, Nanoparticle superlattices as efficient bifunctional electrocatalysts for water splitting, J. Am. Chem. Soc. 137 (2015) 14305–14312.

[14] B. Senthilkumar, Z. Khan, S. Park, K. Kim, H. Ko, Y. Kim, Highly porous graphitic carbon and $Ni_2P_2O_7$ for a high performance aqueous hybrid supercapacitor, J. Mater. Chem. A 3 (2015) 21553–21561.

[15] M. Li, W. Yang, Y. Huang, Y. Yu, Hierarchical mesoporous Co_3O_4@$ZnCo_2O_4$ hybrid nanowire arrays supported on Ni foam for high performance asymmetric supercapacitors, Sci. China Mater. 61 (2018) 1167–1176.

[16] A.R. Selvaraj, R. Rajendiran, D. Chinnadurai, G.R. Kumar, H.-J. Kim, K. Senthil, K. Prabakar, Stabilization of cryptomelane α-MnO_2 nanowires tunnels widths for enhanced electrochemical energy storage, Electrochim. Acta 283 (2018) 1679–1688.

[17] J. Lin, H. Wang, Y. Yan, X. Zheng, H.N. Jia, J. Qi, J. Cao, J. Tu, W. Fei, J. Feng, Core-branched $CoSe_2/Ni_{0.85}Se$ nanotube arrays on Ni foam with remarkable electrochemical performances for hybrid supercapacitors, J. Mater. Chem. A 6 (2018) 19151–19158.

[18] Y. Tang, S. Chen, T. Chen, W. Guo, Y. Li, S. Mu, S. Yu, Y. Zhao, F. Wend, F. Gao, Synthesis of peanut-like hierarchical manganese carbonate microcrystals via magnetically driven self-assembly for high performance asymmetric supercapacitors, J. Mater. Chem. A 5 (2017) 3923–3931.

[19] B. Akinwolemiwa, G.Z. Chen, Fundamental consideration for electrochemical engineering of supercapattery, J. Braz. Chem. Soc. 29 (2018) 960–972.

[20] J. Lin, Z. Zhong, H. Wang, X. Zheng, Y. Wang, J. Qi, J. Cao, W. Fei, Y. Huang, J. Feng, Rational constructing free-standing Se doped nickel-cobalt sulphides nanotubes as battery-type electrode for high-performance supercapattery, J. Power Sources 407 (2018) 6–13.

[21] T.-W. Lin, H.-C. Tsai, T.-Y. Chen, L.–.D. Shao, Facile and controllable one-pot synthesis of hierarchical Co_9S_8 hollow microspheres as high-performance electroactive materials for energy storage and conversion, ChemElectroChem 5 (2018) 137–143.

[22] J. Wen, S. Li, T. Chen, B. Li, L. Xiong, Y. Guo, G. Fang, Porous nanosheet network architecture of CoP@$Ni(OH)_2$ composites for high performance supercapacitors, Electrochim. Acta 258 (2017) 266–273.

[23] L. Jinlong, L. Tongxiang, Y. Meng, K. Suzuki, H. Miura, Comparing different microstructures of CoS formed on bare Ni foam and Ni foam coated graphene and their supercapacitors performance, Colloids Surf. A Physicochem. Eng. Asp. 529 (2017) 57–63.

[24] X. Wei, Y. Li, H. Peng, D. Gao, Y. Ou, Y. Yang, J. Hu, Y. Zhang, P. Xiao, A novel functional material of Co_3O_4/Fe_2O_3 nanocubes derived from a MOF precursor for high-performance electrochemical energy storage and conversion application, Chem. Eng. J. 355 (2019) 336–340.

[25] X.Y. Yu, X.W. Lou, Mixed metal sulfides for electrochemical energy storage and conversion, Adv. Energy Mater. 8 (2018) 1701592.

[26] X. Ma, W. Zhang, Y. Deng, C. Zhong, W. Hu, X. Han, Phase and composition controlled synthesis of cobalt sulfide hollow nanospheres for electrocatalytic water splitting, Nanoscale 10 (2018) 4816–4824.

[27] S. Xie, J. Gou, B. Liu, C. Liu, Synthesis of cobalt-doped nickel sulfide nanomaterials with rich edge sites as high-performance supercapacitor electrode materials, Inorg. Chem. Front. 5 (2018) 1218–1225.

[28] R. Bose, M. Seo, C.-Y. Jung, S.C. Yi, Comparative investigation of the molybdenum sulphide doped with cobalt and selenium towards hydrogen evolution reaction, Electrochim. Acta 271 (2018) 211–219.

[29] B. Liu, S. Qu, Y. Kou, Z. Liu, X. Chen, Y. Wu, X. Han, Y. Deng, W. Hu, C. Zhong, In-situ electrodeposition of cobalt sulfide nanosheet arrays on carbon cloth as a highly efficient bifunctional electrocatalyst for oxygen evolution and reduction reactions, ACS Appl. Mater. Interfaces 10 (2018) 30433–30440.

[30] J. Ning, T. Zhang, Y. He, C. Jia, P. Saha, Q. Cheng, Co_3O_4@CoS core-shell nanosheets on carbon cloth for high performance supercapacitor electrodes, Materials 10 (2017) 608.

[31] N. Li, X. Liu, G.-D. Li, Y. Wu, R. Gao, X. Zou, Vertically grown CoS nanosheets on carbon cloth as efficient hydrogen evolution electrocatalysts, Int. J. Hydrog. Energy 42 (2017) 9914–9921.

[32] W. Xu, M.A. Khan, J. Chen, Y. Long, G. Xu, Y. Bai, X. Zhang, Z. Qiu, S. Lin, D. Fan, The comparative study of electrochemical capacitance performance between sulphur-doped Co_3O_4 and CoS anodes, J. Nanomater. 5676380 (2016) 1–5.

[33] X. Xia, C. Zhu, J. Luo, Z. Zeng, C. Guan, C.F. Ng, H. Zhang, H.J. Fan, Synthesis of free-standing metal sulfide nanoarrays via anion exchange reaction and their electrochemical energy storage application, Small 10 (2014) 766–773.

[34] Z. Xiao, G. Xiao, M. Shi, Y. Zhu, Homogeneously dispersed Co_9S_8 anchored on nitrogen and sulfur co-doped carbon derived from soybean as bifunctional oxygen electrocatalysts and supercapacitors, ACS Appl. Mater. Interfaces 10 (2018) 16436–16448.

[35] B. You, N. Jiang, Y. Sun, Morphology–activity correlation in hydrogen evolution catalyzed by cobalt sulfides, Inorg. Chem. Front. 3 (2016) 279–285.

[36] S. Yuvaraj, S. Layek, S.M. Vidyavathy, S. Yuvaraj, D. Meyrick, R.K. Selvan, Electrical and magnetic properties of spherical $SmFeO_3$ synthesized by aspartic acid assisted combustion method, Mater. Res. Bull. 72 (2015) 77–82.

[37] V.D. Nithya, R.K. Selvan, K. Vediappan, S. Sharmila, C.W. Lee, Molten salt synthesis and characterization of $Li_4Ti_{5-x}Mn_xO_{12}$ (x = 0.0, 0.05 and 0.1) as anodes for Li-ion batteries, Appl. Surf. Sci. 261 (2012) 515–519.

[38] N. Kurra, C. Xia, M.N. Hedhili, H.N. Alshareef, Ternary chalcogenide micro-pseudocapacitors for on-chip energy storage, Chem. Commun. 51 (2015) 10494–10497.

[39] D. Zha, Y. Fu, L. Zhang, J. Zhu, X. Wang, Design and fabrication of highly open nickel cobalt sulfide nanosheets on Ni foam for asymmetric supercapacitors with high energy density and long cycle-life, J. Power Sources 378 (2018) 31–39.

[40] J. Yang, C. Yu, X. Fan, S. Liang, S. Li, H. Huang, Z. Ling, C. Hao, J. Qiu, Electroactive edge site-enriched nickel–cobalt sulfide into graphene frameworks for high performance asymmetric supercapacitors, Energy Environ. Sci. 9 (2016) 1299–1307.

[41] Z. Li, X. Li, L. Xiang, X. Xie, X. Li, D.-R. Xiao, J. Shen, W. Lu, L. Lu, S. Liu, Three-dimensional hierarchical nickel–cobalt–sulfide nanostructures for high performance electrochemical energy storage electrodes, J. Mater. Chem. A 4 (2016) 18335–18341.

[42] Q. Yao, B. Fan, Y. Xiong, C. Jin, Q. Sun, C. Sheng, 3D assembly based on 2D structure of cellulose nanofibril/graphene oxide hybrid aerogel for adsorptive removal of antibiotics in water, Sci. Rep. 7 (2017) 45914.

[43] S. Surendran, R.K. Selvan, Growth and characterization of 3D flower-like β-NiS on carbon cloth: a dexterous and flexible multifunctional electrode for supercapattery and water-splitting applications, Adv. Mater. Interfaces 5 (2018) 1701056.

[44] K.V. Sankar, S.C. Lee, Y. Seo, C. Ray, S. Liu, A. Kundu, S.C. Jun, Binder-free cobalt phosphate one-dimensional nanograsses as ultrahigh-performance cathode material for hybrid supercapacitor applications, J. Power Sources 373 (2018) 211–219.

[45] P. Ganesan, M. Prabu, J. Sanetuntikul, S. Shanmugam, Cobalt sulfide nanoparticles grown on nitrogen and sulfur codoped graphene oxide: an efficient electrocatalyst for oxygen reduction and evolution reactions, ACS Catal. 5 (2015) 3625–3637.

[46] S. Dou, L. Tao, J. Huo, S. Wang, L. Dai, Etched and doped Co_9S_8/graphene hybrid for oxygen electrocatalysis, Energy Environ. Sci. 9 (2016) 1320–1326.

[47] M. Shen, C. Ruan, Y. Chen, C. Jiang, K. Ai, L. Lu, Covalent entrapment of cobalt − iron sulfides in N-doped mesoporous carbon: extraordinary bifunctional electrocatalysts for oxygen reduction and evolution reactions, ACS Appl. Mater. Interfaces 7 (2015) 1207–1218.

[48] H. Xu, J. Cao, C. Shan, B. Wang, P. Xi, W. Liu, Y. Tang, MOF-derived hollow CoS decorated with CeOx nanoparticles for boosting oxygen evolution reaction electrocatalysis, Angew. Chem. Int. Ed. 57 (2018) 8654–8658.

[49] A. Sivanantham, P. Ganesan, S. Shanmugam, Hierarchical $NiCo_2S_4$ nanowire arrays supported on Ni foam: an efficient and durable bifunctional electrocatalyst for oxygen and hydrogen evolution reactions, Adv. Funct. Mater. 26 (2016) 4661.

[50] J. Masa, P. Weide, D. Peeters, I. Sinev, W. Xia, Z. Sun, C. Somsen, M. Muhler, W. Schuhmann, Amorphous cobalt boride (Co_2B) as a highly efficient nonprecious catalyst for electrochemical water splitting: oxygen and hydrogen evolution, Adv. Energy Mater. 6 (2016) 1502313.

[51] P. Chen, K. Xu, Z. Fang, Y. Tong, J. Wu, X. Lu, X. Peng, H. Ding, C. Wu, Y. Xie, Metallic Co_4N porous nanowire arrays activated by surface oxidation as electrocatalysts for the oxygen evolution reaction, Angew. Chem. Int. Ed. 54 (2015) 14710–14714.

[52] J. Lin, H. Wang, X. Zheng, Y. Du, C. Zhao, J. Qi, J. Cao, W. Fei, J. Feng, Controllable synthesis of core-branch Ni_3S_2/Co_9S_8 directly on nickel foam as an efficient bifunctional electrocatalyst for overall water splitting, J. Power Sources 401 (2018) 329–335.

[53] X. Wang, R. Tong, Y. Wang, H. Tao, Z. Zhang, H. Wang, Surface roughening of nickel cobalt phosphide nanowire arrays/Ni-foam for enhanced hydrogen evolution activity, ACS Appl. Mater. Interfaces 8 (2016) 34270–34279.

[54] S. Shit, S. Chhetri, W. Jang, N.C. Murmu, H. Koo, P. Samanta, T. Kuila, Cobalt sulfide/nickel sulfide heterostructure directly grown on nickel foam: an efficient and durable electrocatalyst for overall water splitting application, ACS Appl. Mater. Interfaces 10 (2018) 27712–27722.

[55] M. Zhu, Z. Zhang, H. Zhang, H. Zhang, X. Zhang, L. Zhang, S. Wang, Hydrophilic cobalt sulfide nanosheets as a bifunctional catalyst for oxygen and hydrogen evolution in electrolysis of alkaline aqueous solution, J. Colloid Interface Sci. 509 (2018) 522–528.

[56] N. Wang, L. Li, D. Zhao, X. Kang, Z. Tang, S. Chen, Graphene composites with cobalt sulfide: efficient trifunctional electrocatalysts for oxygen reversible catalysis and hydrogen production in the same electrolyte, Small 13 (2017) 1701025.

[57] Y. Bai, H. Zhang, L. Liu, H. Xu, Y. Wang, Tunable and specific formation of C@

NiCoP peapods with enhanced her activity and lithium storage performance, Chem. Eur. J. 22 (2016) 1021–1029.
[58] K. Xu, H. Cheng, H. Lv, J. Wang, L. Liu, S. Liu, X. Wu, W. Chu, C. Wu, Y. Xie, Controllable surface reorganization engineering on cobalt phosphide nanowire arrays for efficient alkaline hydrogen evolution reaction, Adv. Mater. 30 (2018) 1703322.
[59] Z. Khan, B. Senthilkumar, S.O. Park, S. Park, J. Yang, J.H. Lee, H. Song, Y. Kim, S.K. Kwak, H. Ko, Carambola-shaped VO_2 nanostructures: a binder-free air electrode for an aqueous Na–air battery, J. Mater. Chem. A 5 (2017) 2037–2044.
[60] J. Liu, J. Wang, Z. Ku, H. Wang, S. Chen, L. Zhang, J. Lin, Z.X. Shen, Aqueous rechargeable alkaline $Co_xNi_{2-x}S_2/TiO_2$ battery, ACS Nano 10 (2016) 1007–1016.
[61] J. Liu, M. Chen, L. Zhang, J. Jiang, J. Yan, Y. Huang, J. Lin, H.J. Fan, Z.X. Shen, A flexible alkaline rechargeable Ni/Fe battery based on graphene foam/carbon nanotubes hybrid film, Nano Lett. 14 (2014) 7180–7187.
[62] Y. Tang, T. Chen, S. Yu, Y. Qiao, S. Mu, S. Zhang, Y. Zhao, L. Hou, W. Huang, F. Gao, A highly electronic conductive cobalt nickel sulphide dendrite/quasispherical nanocomposite for a supercapacitor electrode with ultrahigh areal specific capacitance, J. Power Sources 295 (2015) 314–322.
[63] J. Zhu, L. Xiang, D. Xi, Y. Zhou, J. Yang, One-step hydrothermal synthesis of flower-like CoS hierarchitectures for application in supercapacitors, J. Bull. Mater. Sci. (2018) 54.
[64] H. Chen, J. Jiang, Y. Zhao, L. Zhang, D. Guo, D. Xia, One-pot synthesis of porous nickel cobalt sulphides: tuning the composition for superior pseudocapacitance, J. Mater. Chem. A 3 (2015) 428–437.
[65] H. Zhang, B. Guan, J. Gu, Y. Li, C. Ma, J. Zhao, T. Wang, C. Cheng, One-step synthesis of nickel cobalt sulphides particles: tuning the composition for high performance supercapacitors, RSC Adv. 6 (2016) 58916–58924.
[66] Y. Subramanian, G.K. Veerasubramani, M.-S. Park, D.-W. Kim, Investigation of Layer Structured NbSe2 as an Intercalation Anode Material for Sodium-Ion Hybrid Capacitors, J. Electrochem. Soc. 166 (4) (2019) A598–A604, https://doi.org/10.1149/2.0641904jes.
[67] H. Wang, C. Wang, C. Qing, D. Sun, B. Wang, G. Qu, M. Sun, Y. Tang, Construction of carbon-nickel cobalt sulphide hetero-structured arrays on nickel foam for high performance asymmetric supercapacitors, Electrochim. Acta 174 (2015) 1104–1112.
[68] S.J. Patil, J.H. Kim, D.W. Lee, Graphene-nanosheet wrapped cobalt sulphide as a binder free hybrid electrode for asymmetric solid-state supercapacitor, J. Power Sources 342 (2017) 652–665.
[69] F. Wang, G. Li, J. Zheng, J. Ma, C. Yang, Q. Wang, Microwave synthesis of three-dimensional nickel cobalt sulfide nanosheets grown on nickel foam for high-performance asymmetric supercapacitors, J. Colloid Interface Sci. 516 (2018) 48–56.
[70] Y. Hu, M. Liu, Y. Hu, Q. Yang, L. Kong, L. Kang, One-pot hydrothermal synthesis of porous nickel cobalt phosphides with high conductivity for advanced energy conversion and storage, Electrochim. Acta 215 (2016) 114–125.